Open Access Articles

Printed Oxide Thin Film Transistors: A Mini Review

Citation	Choi, C. H., Lin, L. Y., Cheng, C. C., & Chang, C. H. (2015). Printed Oxide Thin Film Transistors: A Mini Review. ECS Journal of Solid State Science and Technology, 4(4), P3044-P3051. doi:10.1149/2.0071504jss
DOI	10.1149/2.0071504jss
Publisher	Electrochemical Society
Version	Version of Record
Terms of Use	http://cdss.library.oregonstate.edu/sa-termsofuse

Printed Oxide Thin Film Transistors: A Mini Review

Chang-Ho Choi,[a] Liang-Yu Lin,[b] Chun-Cheng Cheng,[b] and Chih-hung Chang[a],*,[z]

[a]*Oregon Process Innovation Center/Microproduct Breakthrough Institute and School of Chemical, Biological & Environmental Engineering, Oregon State University, Corvallis, Oregon 97331, USA*
[b]*AU Optronics Corporation, Hsinchu Science Park, Hsinchu, Taiwan*

Compared to conventional amorphous silicon (a-Si) TFTs, amorphous metal oxide TFTs have superior device performance such as higher mobility, better sub-threshold swing, and lower off-state current. Amorphous metal oxide TFTs have an additional advantage on the device uniformity due to the lack of grain boundary issues in the poly-Si TFTs. Compared with sputtered oxide TFTs, metal oxide TFTs with solution processes have better flexibility and controllability to adjust the composition of chemical solution. Among various solution-based approaches, direct printing is a promising low-cost technique in fabricating TFTs. The printing technique offers several advantages in manufacturing electronics such as a direct writing of materials, reduction of chemical waste, and reproducibility with high-resolution scale, which are not affordable from other solution-based approaches. While many printed OTFTs have been reported, relatively fewer studies, associated with printed metal oxide TFTs, have been pursued. Interests to printed metal oxide TFTs have grown continuously since the first report of a general route toward printed oxide TFTs. A variety of metal oxide materials have been reported as the channel layer of printed metal oxide TFTs. In this mini review paper, the development of printed metal oxide TFTs was discussed including the ink formulations, the types and characteristics of the applied printers, and fabricated thin film transistor characteristics. Lastly the review is concluded with a concise summary and future outlook from an industry perspective.

Thin film transistors (TFTs), first reported by Lilienfeld and Heil almost nine decades ago, have continuously being developed and improved for low cost electronic switches.[1,2] Advanced fabrication techniques and materials expand its application to low cost, large size, high resolution, and high-speed flat panel displays.[3] The greatest advancement was accompanied with the advent of a-Si:H as a semiconductor channel layer.[4] Although a-Si:H semiconductor exhibited lower electronic properties (carrier mobility $\leq$ 1 cm^2/Vs) than TFTs based on polycrystalline channel layers (e.g. CdS), the electronic transport properties of a-Si:H were sufficient as switching elements in Liquid Crystal Displays, along with other benefits such as lower cost, high uniformity and excellent reproducibility in large area fabrication. However, lower performances of a-Si:H TFTs limit its application in AMOLED display. Metal oxide semiconductors have been intensively researched over the past decade due to their superior electrical properties including high carrier mobility ($\sim$1– 100 cm^2/Vs), high optical transparency, good thermal/environmental durability, and potentially low-manufacturing cost.[5,6] Significant progress of metal oxide TFTs has demonstrated the advantages over a-Si:H TFTs as next candidate for high-performance display applications.[7,8]

In terms of manufacturing metal oxide semiconductors as the active channel layers in TFTs, gas-phase deposition technique that requires high vacuum facilities has been primarily employed, which involves higher capital and operation cost. Recently, metal oxide TFTs fabricated via solution-based processes have been considerably pursued for their potentials of offering simplicity, low cost, high throughput, and large area deposition.[9–11] Among various solution-based approaches, direct printing is a promising low-cost technique in fabricating TFTs. The printing technique offers several advantages in manufacturing electronics such as a direct writing of materials, reduction of chemical waste, and reproducibility with high-resolution scale, which are not affordable from other solution-based approaches. Especially for the TFTs fabrication, printing can significantly simplify manufacturing processes by directly defining the channel area, the gate, and the source and drain contacts. Photolithography processes, essential in conventional spray coating and spin-coating, are not required in printing, allowing for much low costs and high throughput manufacture of TFTs.

Printing, considering one of the main advantages, has been actively pursued in fabricating components of organic TFTs (OTFTs) such as the active channel layer and source/drain electrodes. For instance, the fabrication of all-polymer transistor was reported by Sirringhaus et al. by combining inkjet printing and photolithography technique.[12] In order to define the 5 μm active channel layer, water-soluble inks containing materials for source and drain electrodes were first printed onto hydrophilic substrates, and their spreading was then confined by hydrophobic barriers prepared by photolithography. They also explored dewetting behavior of conducting polymer inkjet droplets on patterned surfaces to understand influential factors on dewetting.[13] Paul et al. fabricated coplanar structured OTFT, printing polymer semiconductor channel layer onto patterned source and drain electrode.[14] Arias et al. reported the fabrication of all inkjet-printed polymer TFTs.[15] They used only inkjet printing for depositing and patterning without the help of any lithography technique in the entire TFT manufacturing process. The TFT fabrication with printable carbon nanotube (CNT) was reported by Beecher et al.[16] The authors explored CNT ink preparations to find the optimal ink conditions.

While many printed OTFTs have been reported, relatively few studies, associated with printed metal oxide TFTs, have been pursued before the report by Lee et al.[17] Interests to printed metal oxide TFTs have grown continuously since then, yielding an increasing number of relevant publications. A variety of metal oxide materials have been reported as the channel layer of printed metal oxide TFTs, and at the same time proper ink preparation methods and tailored droplet patterning were discussed. Types of printer used for the fabrication of metal oxide TFTs also varied upon the ink fluid properties and device applications. In this mini review, we will introduce the type of printers, commonly used for fabricating metal oxide TFTs, focusing on printer characteristics and working principles. And then we will review developments of printed metal oxide TFTs, dealing with the ink formulation and critical printing parameters. Lastly we will conclude with a concise summary and future outlook.

*Electrochemical Society Active Member.
[z]E-mail: Chih-hung.Chang@oregonstate.edu

Types of Printer

Thermal and piezoelectric inkjet printer.— The most common printer used for fabricating metal oxide TFTs is inkjet printer. Inkjet printer is also commonly used at home and office environment to print high quality image on papers. Inkjet printer mainly consists of the print head and ink reservoir. The ink fluid is stored in the reservoir and ejected through jetting nozzles in the print head. The key components of the print head are nozzles whose size range from micrometer to sub-micrometer in diameter to deliver the high accuracy of resolution. The array of nozzles are mounted on a single planar sheet of a material and formed as orifices. The assembly of the print head and reservoir move back and forth with a certain velocity, jetting ink fluid on substrate. Inkjet printer can be divided into continuous ink jet (CIJ) and drop on demand (DOD) inkjet upon the type of jetting. Since most of reported metal oxides TFTs are introduced through the DOD inkjet, we will focus on the DOD inkjet. Ink is ejected from nozzles by imposing a pulse of force to the ink in the supply tube, and type of the applied forces can be either thermal or piezoelectric, which in turn splits the DOD inkjet into either thermal inkjet or piezoelectric inkjet. The schematic diagrams of both inkjet printers are shown in Figure 1. In the thermal inkjet printer,[18] the main components include the ink channel, photoimageable polymer, resistive metallic layer, thin film conductor, and orifice plate. The ink channel is built on the surface of a silicon substrate with a photoimageable polymer. A small heater with less than 1 μm thickness serves as a thin film resistive metallic layer in the wall of the ink channel. A pulse of electrical current flows through the heater for approximately 1 μs in duration. The ink ejection in the thermal ink jet printer can be accomplished through several processes, including bubble nucleation, bubble growth, bubble collapse, and ink refill in sequence. The sufficient electrical current is provided to the heater to boil the ink explosively, creating the bubble nucleation. The bubble grows very quickly, expanding about 1000 times in volume. The ink is ejected toward the substrate as the rapid bubble expansion causes a pressure pulse in the ink fluid. After the ejection of the ink, the bubble immediately collapses. Lastly the ink from the reservoir is transported into the nozzle due to the surface tension of the ink meniscus in the nozzle for the subsequent ink ejection toward the substrate.

In the piezoelectric printer,[19] instead of using the heater, piezoelectric materials are used to induce the ink ejection. As high electric field is supplied to the piezoelectric materials, they deform and squeeze the ink channel, resulting in the creation of a pressure pulse and the ink ejection toward the substrate. An elastic diaphragm separates the piezoelectric materials from the ink, and the laminated metal plates are commonly used to build the ink channel.

Gravure and flexographic printer.— Like engraving, gravure printer is a form of intaglio printing.[20] It is capable of producing high-resolution patterns with relatively high throughput. The working principle of the gravure printer is displayed in Figure 1c. With gravure printing a pattern is fabricated on the surface of a metal plate or cylinder so that the targeted pattern is in the recesses of the plate. The recesses are filled with ink and the raised portions of the plate or cylinder are free of ink leaving the ink only in the recesses. The blade is set up and scrapes the excess amount of the ink to apply the proper amount of the ink to the substrate. The substrate is pressed against the inked plate or cylinder when the substrate is sandwiched between the inked cylinder and impression roller and the image is transferred to the substrate. It has not been widely used for printed oxide TFTs perhaps due to the high cost of plate making.

Similar to rubber stamping, flexographic printing is one of the most basic forms of printing.[21,22] It has been frequently used for printing on plastic foils, acetate films and papers used in packaging. It relies on printing plates made of flexible polymers. The inked plates with a raised pattern are rotated on a cylinder, which transfers the inks onto the substrate (Figure 1d). Flexographic printing is a high-speed print process and can print on many types of substrate materials.

Transfer printing.— Transfer printing involves transferring targeted materials such as metal, polymer, and semiconductor onto a substrate by utilizing the surface adhesion force.[23,24] The material adhered onto a transfer substrate with low surface adhesion is transferred to a device substrate with higher surface adhesion (Figure 2a). Therefore, the proper selection of substrates with different adhesion forces should be carefully made to achieve the successful material
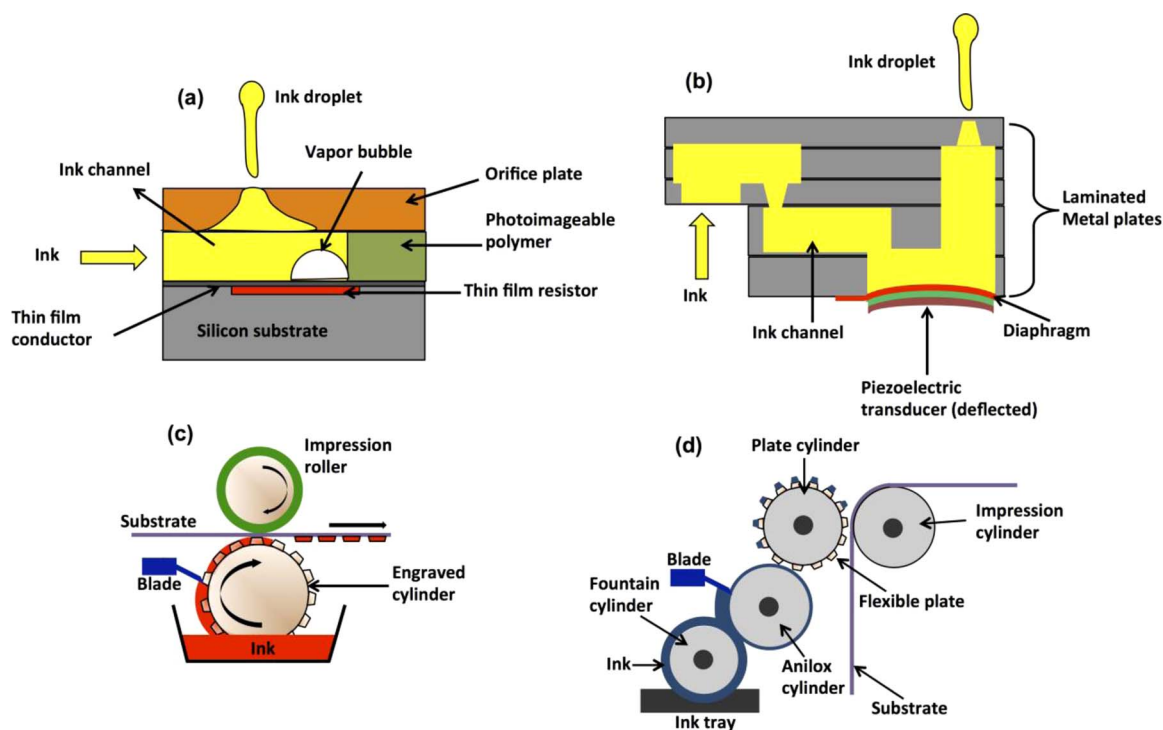

Figure 1. Schematic diagram of (a) thermal inkjet printer (b) piezoelectric inkjet printer (c) gravure printer and (d) flexographic printer.

ECS Journal of Solid State Science and Technology, **4** (4) P3044-P3051 (2015)
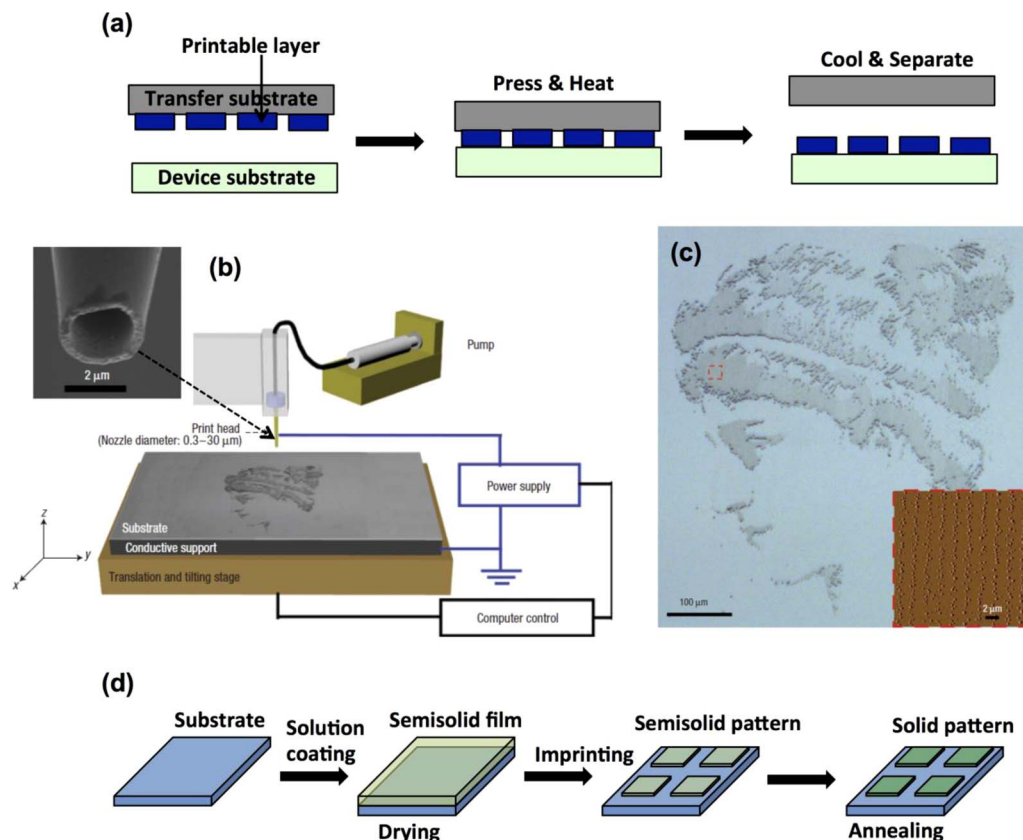

Figure 2. Schematic diagram of (a) transfer printing (b) electrohydrodynamic printer (c) feature composed of nanometer sized dots (d) rheology printing. (Reproduced from Nature Publishing Group with permission.)

transferring to the device substrate. To promote the transferring, surface treatments of substrates are frequently applied. The heat and pressure can also be used for facilitating transfer printing.

High resolution printing.— Although both thermal and piezoelectric inkjet printer are capable of producing micron-sized features, some drawbacks such as resolution limitation and droplet deviation drive development of printers, capable of patterning sub-micron features. Park et al. reported high-resolution electrohydrodynamic jet printing, capable of creating printing features within sub-micrometer range.[25] The components of the printer are displayed in Figure 2b. A syringe pump was used to supply inks to the nozzle fabricated with a gold-coated capillary glass tube. As electrical fields, generated by a power supply, were applied between the conductive nozzle and a conducting support substrate, an electrohydrodynamic flow was created, leading to ejection of fluid inks toward the substrate. Printing of complex patterns were achieved by incorporating a computer-controlled x, y, and z axis stage and graphic software. By adopting the capillary glass tube of 300 nm diameter and optimizing process conditions, they were able to produce complex patterns comprising a number of nanometer sized dots (Figure 2c).

Another important aspect of printing technique is the ability to accurately pattern features with well-defined shapes. Keneda et al. reported rheology printing for metal-oxide patterns within sub-micrometer range.[26] The printing processes follow well-known imprinting technique that consists of drying, imprinting, etching residual film, and annealing process in sequence (Figure 2d). By selecting appropriate metal-organic precursors that form "physical gel" at glass transition temperature, the authors fabricated submicron-sized patterns without the significant deformation of patterned features during the post-annealing. This made their approach distinct from common imprint techniques that generally experience a large shrinkage of pattern during the post-annealing.[27] Based on results of various char-

acterizations, they indicated that the physical gel of metal-organic precursors, formed after drying, showed rheological properties and underwent substantial transformation to metal-oxide-metal skeleton during thermal imprinting process.

Patterning nanometer-sized features by utilizing surface energy (dewetting) was proposed by Wang et al.[13,28] They demonstrated this concept by fabricating organic TFTs and also explored important process parameters that affect the pattering. Sub-micrometer lines with width range from 250 nm to 20 μm was formed on the SiO$_2$/Si substrate through electron beam lithography (EBL), followed by a subsequent surface treatment with hydrophobic self-assembled monolayer (SAM). The ink containing aqueous PEDOT/PSS was printed onto the pre-patterned hydrophobic line, and the ink droplet split into two droplets across the hydrophobic line during the drying of the ink. These two droplets served as source and drain electrodes for a transistor. By subsequently depositing organic active channel layer onto the pre-patterned layer, the active channel length with sub-micrometer size was defined. The gate electrode was formed, printing the PEDOT/PSS ink on the channel layer again. Although the EBL technique and other processes were required for the patterning, it offers the new concept to fabricating sub-micrometer features.

Development of Printed Metal Oxide TFTs

Lee et al. reported a general route toward printable multicomponent metal oxide semiconductors, based on metal halide precursors dissolved in an organic aprotic solvent.[17] They prepared the ink fluid by dissolving metal halide precursors in acetonitrile, an organic aprotic solvent that will not hydrolyze the metal halide precursors. A modified HP desktop thermal inkjet printer was used for their study. Smooth and uniform metal halide films were obtained, and these films were converted to metal-oxide-metal frame after a thermal annealing process. The detailed mechanism of the metal oxide formation from
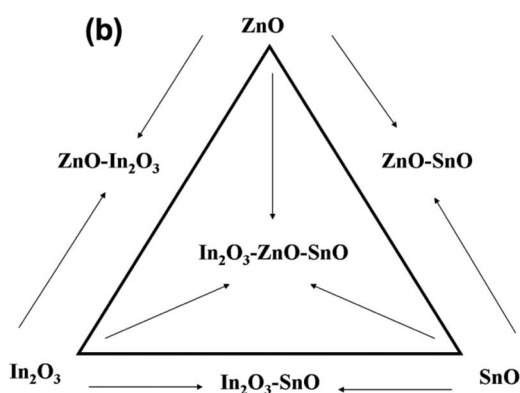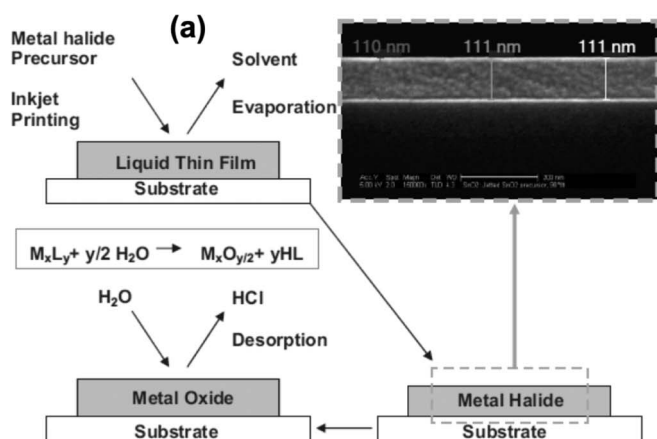
Figure 3. Formation mechanism of metal oxide film and cross sectional SEM image of printed metal halide precursor film (b) and first reported printed multicomponent metal oxide materials. (Reproduced from Wiley-VCH with permission.)

metal halide was illustrated in Figure 3a. Printed metal halide film absorbed H_2O in the air, which in turn formed metal hydroxyl halide film. During the thermal annealing step, the metal hydroxyl halide film was transformed to metal oxide through the removal of volatile by-product such as HCl. The authors fabricated IZO TFTs by using this ink fluid and reported the device performances, which are comparable with those of the spin-coated one, with a mobility of 7.4 cm²/Vs, on-off ratio of 10^4, and $V_{on} = -26$ V. A variety of transparent semi-conductor oxide thin films including ZnO, In_2O_3, SnO_2, $ZnO-In_2O_3$ (ZIO), $In_2O_3-SnO_2$ (ITO), $ZnO-SnO_2$ (ZTO), and $In_2O_3-ZnO-SnO_2$ (IZTO) have been fabricated in our laboratory using this new process by combining simple $ZnCl_2$, $SnCl_2$ (or $SnCl_4$), and $InCl_3$ precursors in acetonitrile by using both inkjet printing and spin-coating including an ink-jet-printed IZTO MISFET with a field-effect mobility of 3.9 cm² /Vs and a drain-current on-to-off ratio of approximately 10^6 with a positive turn-on voltage of 1 V. Using $SnCl_4$ precursor, Lee et al. also reported porous SnO_2 TFTs fabricated by inkjet printing.[29] They proposed that the porous structure was originated from the evolution of HCl gas during the fast thermal annealing process (500 °C in the air). Despite the large portion of porosity inside the film, the film was still continuous and offered the electron paths for a transistor. A field effect mobility of 3.62 cm²/Vs, on-off ratio of 10^3, and $V_{on} = -39$ V was reported. The porous structure could potentially useful for sensing applications.

With the addition of ethylene glycol to adjust the viscosity and surface tension, a variety of printed metal oxide TFTs have been reported using piezoelectric inkjet printer including binary oxides (ZnO, In_2O_3, SnO_2, Ga_2O_3), ternary oxides (ZIO, ITO, ZTO, IGO) and quaternary compounds (IZTO, IGZO).[30,31] The IZTO TFTs, prepared at 600 °C for 1 hr. in the air condition, showed a mobility of 30 cm²/Vs, on-off ratio of 10^6, and $V_{on} = -39$ V.[30] The same annealing conditions were applied for the fabrication of the IGO TFTs, and device performances with a mobility of 5.5 cm²/Vs, on-off ratio of 10^5, and $V_{on} = -21$V were reported.[31] These results offered strong evidence that metal halide-based precursor inks fluid offer an avenue to form patterned metal oxide semiconductors through a simple and low-cost process and to fabricate high performance transparent thin film electronics. Since the introduction of the printed metal oxide TFTs, associated with metal halide precursor inks, many researchers have adopted and improved this approach, attempting to expand types of metal oxide materials, seek more effective ink formulation, and optimize printing and post processing parameters. Kim et al. fabricated ZTO TFTs by printing ZTO channel layer using a piezoelectric inkjet printer.[32] The substrate temperature was varied to investigate its effect on the device performances. Figure 4 shows the printing patterns of ZTO films and the corresponding transfer characteristic curves of TFTs. The substrate temperature had a significant influence on both the field effect mobility and threshold voltage (V_{th}). The authors correlated the temperature dependence of the device performances with the morphology of the films. Due to the Maragoni flow that is responsible for the creation of coffee-ring patterns, all of the ink droplets have the coffee-ring patterns regardless of the substrate temperature.[33] It is generally known that the higher temperature tends to shrink the droplet size, but increase the droplet thickness, particularly near
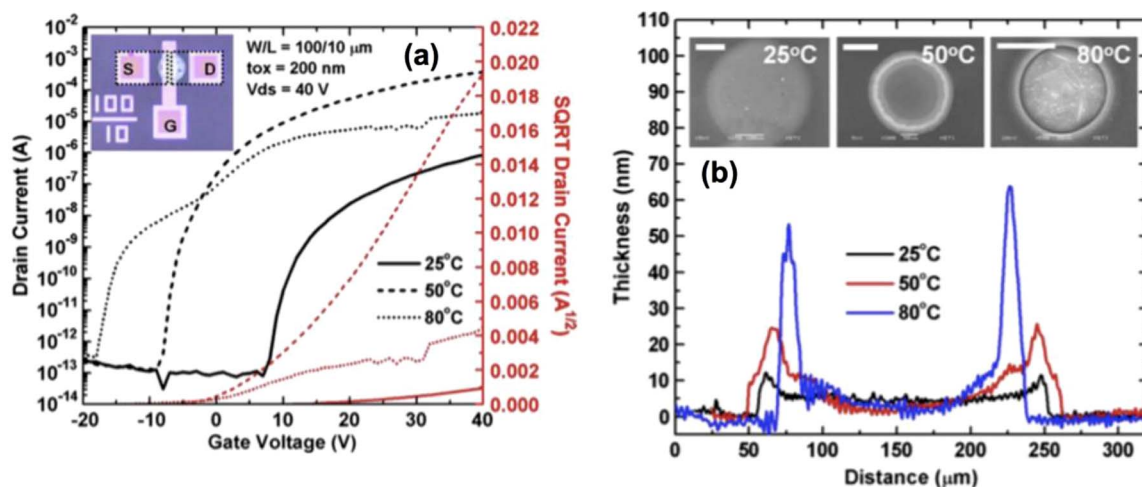

Figure 4. Transfer characteristics of printed ZTO TFTs fabricated at various substrate temperatures (a) and characterization of relevant ink droplets (b). (Reproduced from IEEE with permission.)
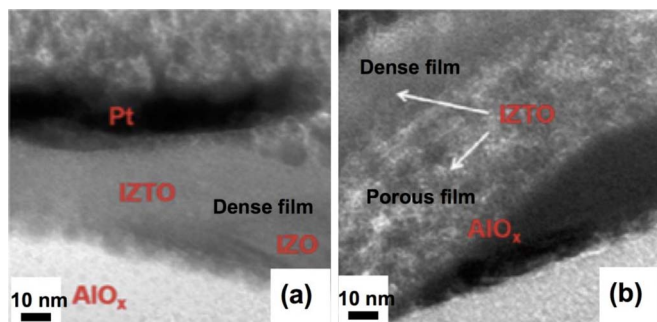
Figure 5. SEM images of printed IZTO films: (a) dense film with 35 nm thickness and (b) two layers porous film with 85 nm thickness. (Reproduced from ACS Publications with permission.)

peripheral area of the droplet.[34] These phenomena were also observed in the printed ZTO TFTs as shown in Figure 4b. After finding the optimal substrate temperature in which the optimal film morphology was obtained, the authors were able to acquire the device performances (mobility = 4.98 cm^2/Vs, on-off ratio = 1.5×10^9, and V_{th} = 8.6 V).

Avis et al. were able to control the film thickness of printed IZTO thin film by varying the substrate temperature and reported the film thickness effects on device performances.[35] By using Al_2O_3 dielectric layer processed by a spin-coating method and finding the optimal film thickness, they achieved an impressive mobility of $\sim$110 cm^2/Vs (Figure 5a). In the printing process, as the film thickness increased, the film morphology deteriorated, creating a porous film structure (Figure 5b). They related the cause of the porous structure formation to the evolution of HCl gas during the annealing process, as reported previously by Lee et al.[29] for the fabrication of porous SnO_x films. They also observed a two-layer IZTO film structure from films thicker than 85 nm as shown in Figure 5b. Both the pore creation and two layer formations resulted in the decline of the device performances.

Garlapati et al. reported In_2O_3 TFTs, composed of a printed crystalline In_2O_3 channel layer and a polymer electrolyte dielectric layer.[36] They annealed the TFTs at various temperatures in the air to study their effects on the device performances. All of the printed films had high surface roughness, and at a low temperature an incomplete oxide formation occurred. In spite of the non-optimized film quality, In_2O_3 TFTs operated excellently, showing a mobility of 126 cm^2/Vs, on-off ratio of 2×10^7, and V_{th} = 0.37 V. The authors attributed the superior device performances to the compatibility of the polymer electrolyte to rough In_2O_3 channel layer. Given excellent device performances obtained at mild annealing temperature, they also addressed the important role of the polymer electrolyte dielectric layer in fabricating low temperature printed metal oxide TFTs.

Jeong et al. derived similar ink formulation approach from the metal halide precursor ink formulation, with the aim of avoiding the formation of toxic by-products (i.e. HCl gas).[37] They used metal salts formulated with nitrate or acetate derivative instead of using metal halide salts, and these metal salts were dissolved in 2-methoxyethanol (2-ME) to form the ink fluid. The printed film is subjected to the annealing process at high temperature to remove organic compounds and promote the metal oxide formation, as described in the metal halide ink printing. Kim et al. first demonstrated ZTO TFTs printed by using the metal salt precursor ink.[38] In particular the authors modified the surface energy of the substrate by treating the surface with different chemicals prior to the printing. These treated surfaces displayed the different wettability to the ink fluid, and the highest device performance was obtained from the surface to show high wettability. The authors also studied the substrate temperature dependence of the film thickness. Jeong et al. discussed the device stability of printed ZTO TFTs.[39] The devices were found to be not as stable as the spin-coated counterparts, yielding a large positive shift of the threshold voltage under a positive bias stress. They claimed that this stability issue resulted from a creation of nanopores during the annealing process. In addition to the printed ZTO TFTs, many researchers have focused on printed

IGZO TFTs.[40,41] Precursor compositions for the IGZO film formation varied upon the types of applied printer and chemistry of the ink formulation, indicating that optimizing printing process is necessary for its own case study. Wang et al. investigated an influence of the channel thickness on printed IGZO TFTs.[42] They found the optimal film thickness by controlling the number of the printing and obtained the highest mobility of 1.41 cm^2/Vs. Additionally they studied the contact resistance issue between IGZO channel layer and ITO source/drain electrodes.[43] By inserting a printed IZO layer between the channel layer and electrodes, they were able to reduce contact resistance and improve the mobility by approximately three times. Hennek et al. also put an emphasis on reducing the contact resistance to yield the high performance IGZO TFTs.[44] The authors investigated the contact resistance effects on the device performances by changing the transistor structure and found that bottom-gate top-contact (BGTC) TFTs significantly reduced the contact resistance, compared with bottom-gate bottom-contact (BGBC) TFTs. This reduced contact resistance led to the mobility of 2.5 cm^2/Vs. Jeong et al. discussed the role of ethylene glycol additive as an ink fluid component in improving printed IGZO TFTs.[45] They demonstrated that EG served as a bridging chelating ligand in precursor solutions, and with its high boiling point (198 $^\circ$C), it made the ink fluid suitable for the printing without clogging nozzles. They also claimed that EG facilitated the metal-oxide-metal formation, while suppressing metal-hydroxide structure, offering excellent electron paths in dispersed vacant s-states. Furthermore, by using ITO source/drain electrodes, they were able to improve the device performances, with a mobility of 7.6 cm^2/Vs and on-off ration of 10^7.

In an effort to lower down the processing temperature, Meyers et al.[46] reported the design and synthesis of an ink based on zinc complex ions, $Zn(OH)_x(NH_3)_y^{(2-x)+}$ in water and isopropanol solution. A modified HP thermal inkjet printer was used for their study. They successfully converted the inkjet printed precursor film into dense and uniform ZnO films at an annealing temperature as low as 150 $^\circ$C in flowing nitrogen condition. The resulting transistors exhibited a mobility of 0.4 cm^2/Vs and on-off ratio of 10^6, and the device performances were further improved at higher annealing temperature (300 $^\circ$C), with a mobility of 4.3 cm^2/Vs, and on-off ratio of $>10^6$.

So far, metal oxide TFTs, manufactured by either thermal or piezo-electric inkjet printer, have been discussed. There have been some reports regarding the fabrication of printed metal oxide TFTs using different types of printers, including the aforementioned high-resolution printing techniques. We will discuss the development of TFTs fabricated by these printing techniques. Lee et al. used the electrohydrodynamic (EHD) jet printing to fabricate IZO TFTs (Figure 6a–6c).[47] After optimizing the ink fluid composition, they employed the EHD printer to print the IZO channel layer for the fabrication of printed IZO TFTs. They also fabricated invisible printed IZO TFTs, with a visible transparency value larger than 88%. The device performances showed the mobility of 32 cm^2/Vs with the use of high k HfO_2 dielectric layer. The EHD printer was also used for the fabrication of ZTO TFTs by Lee et al.[48] Key printing parameters were explored, and after optimizing the printing process and ink formulation, they were able to fabricate the high performance printed ZTO TFTs, showing a mobility as high as 9.82 cm^2/Vs, on-off ratio of 3.7×10^6, and a threshold voltage of 2.36 V. Jeong et al. demonstrated the enhanced device performances and bias stability of EHD-printed IZGO TFTs by developing the ink formulation.[49] They added formamide (FA) solvent as a co-solvent in preparing the ink fluid and claimed that the FA incorporation into the ink fluid led to reducing hydroxide contents and facilitating the oxygen vacancy formation. Fabricating the IZGO TFTs by the EHD printer evidenced the role of the FA solvent, showing a mobility of 1.3 cm^2/Vs.

Kaneda et al. fabricated In_2O_3 and IZO TFTs using the rheology printing.[26] Instead of directly printing the channel layer, the printing was applied to make patterning of source/drain/gate electrodes, followed by the channel layer deposition by a spin-coating process. The channel length of 0.5 μm was defined by the rheology printing with high accuracy.
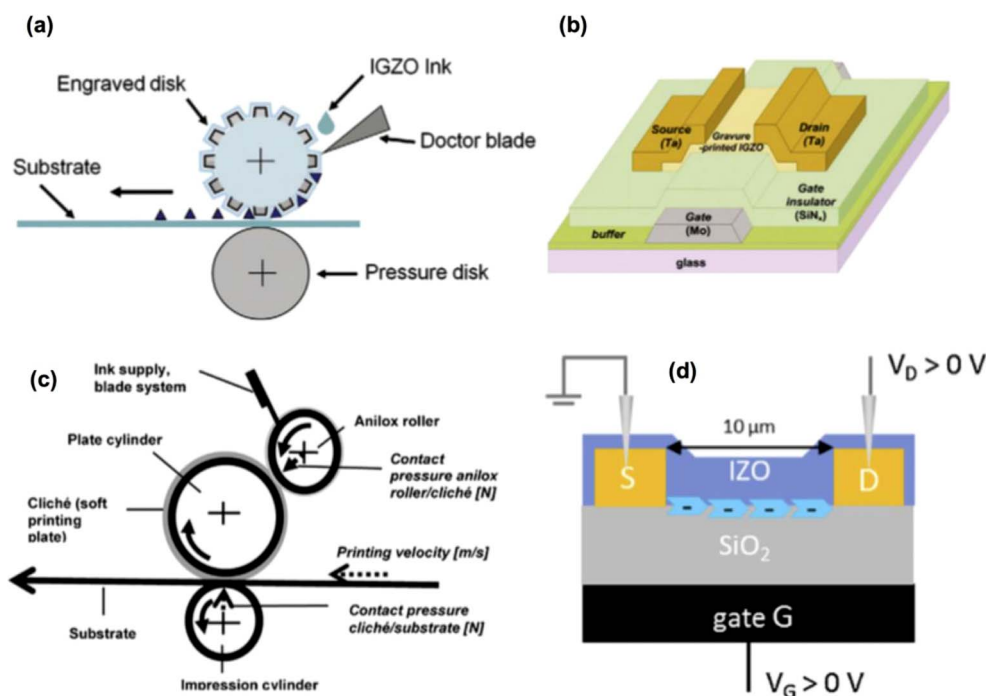
Figure 6. (a) Schematic diagram of gravure printing process and (b) schematic structure of the resulting IGZO TFT (c) Schematic diagram of flexographic printing process for IZO and (d) printed IZO TFTs. (Reproduced from Elsevier with permission.)

Dilfer et al. reported flexographic printed IZO TFTs (Figure 7c and 7d).[50] It was revealed that printed IZO film thickness strongly depends on printing parameters, and the optimal printing parameters offered a good device performances, with a mobility of 2.4 cm²/Vs, on-off ratio of 5.2×10^7, and threshold voltage of 4 V. Choi et al. used a gravure printer to fabricate IGZO TFTs.[51] Printing processes were optimized, and the device performance were reported, with a mobility of 0.81 cm²/Vs and on-off ratio of 1.36×10^6.

Another approach to printable metal oxide semiconductors is to use metal oxide nanocrystals. The inherent advantage of this approach for achieving the low temperature fabrication of printed metal oxide TFTs is the use of precursors consisting of preformed metal oxide semiconductor nanocrystals. So far, only binary compounds such as ZnO and In_2O_3 inks have been reported due to the difficulty of synthesizing multicomponent oxide nanoparticles. Liu et al. fabricated printed ZnO TFTs by using dispersed ZnO nanoparticles in organic solvents.[52] The printed film was subsequently annealed at 200 °C in a reducing atmosphere to decompose organic compounds and other by-products. They reported a ZnO thin film transistor with a mobility of 0.69 cm²/Vs and a low on-off ratio of 4×10^1 due to the poor morphology of the film.
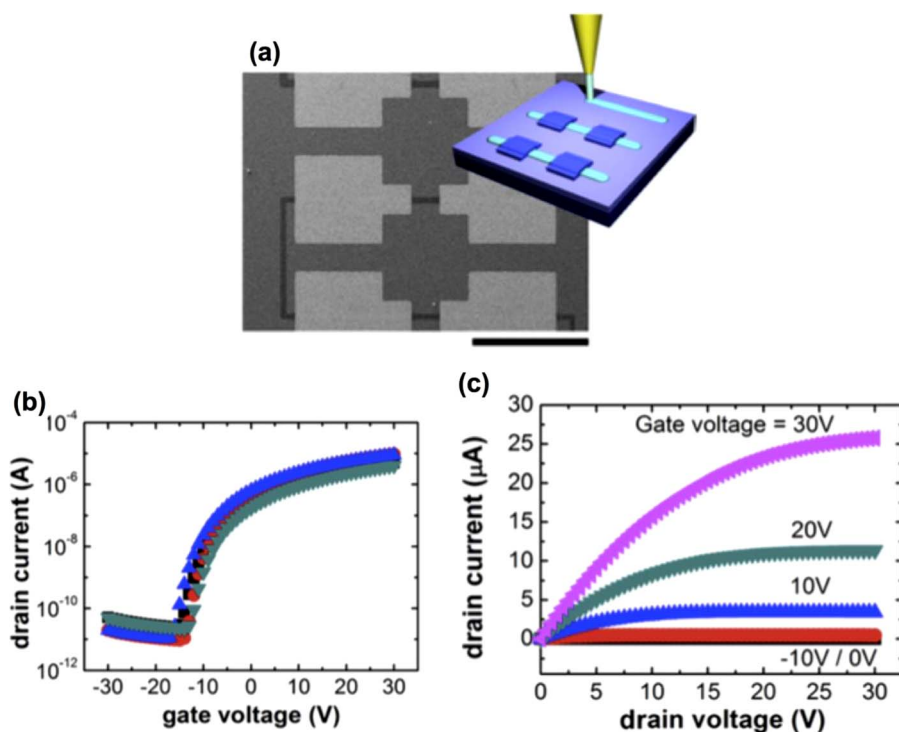

Figure 7. (a) SEM image of EHD-printed IZO TFTs and (b) transfer (c) output characteristics. (Reproduced from AIP Publishing LLC with permission.)
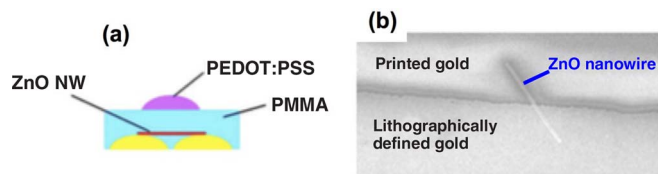
Figure 8. Scheme of ZnO NW TFT structure (a) and TEM image of SEM image of single ZnO NW placed between electrodes. (Reproduced from AIP Publishing LLC with permission.)
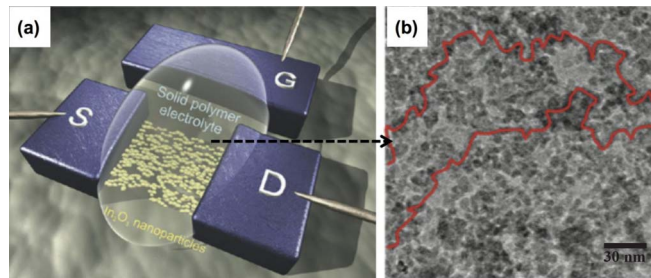

Figure 9. Scheme of printed In 2O3 TFTs (a) and TEM image of channel layer (red line is for a clear visualization of the percolation path). (Reproduced from ACS Publications with permission.)

Noh et al. demonstrated the patterning ability of tailored surface energy (self-aligned inkjet printing) by fabricating ZnO nanowire (NW) TFTs (Figure 8a).[53] The ZnO NW, synthesized by thermal chemical vapor deposition, were dispersed in hydrophilic solvents for the ink formulation and jetted onto the pre-defined source/drain electrodes whose surface were chemically treated that the surface possessed hydrophobic properties (Figure 8b). The ZnO NW channel length, defined by the distance between electrodes, showed the decent device performances, with a mobility of 2–4 cm^2/Vs and on-off ratio of 10^4.

Dasgupta et al. reported the fabrication of printed In$_2$O$_3$ TFTs using dispersed In$_2$O$_3$ nanoparticles at room temperature (Figure 9a).[54] Although the printed In$_2$O$_3$ thin film was not thermally annealed to remove the organic stabilizers, the authors indicated that the percolation path for charge carriers could be established since In$_2$O$_3$ nanoparticles, partially covered with the stabilizers, form a solid-solid contact as evidenced in the TEM image (Figure 9b). By printing a solid polymer electrolyte as the dielectric layer, they were able to fabricate In$_2$O$_3$ TFTs on a flexible substrate and achieve a mobility of 0.8 cm^2/Vs.

Another interesting approach is reported by, Eun et al.[55] who fabricated flexible and transparent ZnO TFTs on PET substrate using transfer printing method. The transparent thin film transistors were fabricated using ZnO, SiO$_2$ and ITO as the channel, insulator, gate, source and drain by vapor phase deposition techniques on silicon wafer with a Ge sacrificial layer. The ZnO TFTs were picked up by a PDMS stamp after dissolving the sacrificial layer and transfer to PET substrate. The ZnO TFTs showed excellent mechanical reliability during the 2000 cycles of the bending fatigue test.

Summary and Future Directions

In this mini review paper, the development of printed metal oxide TFTs was discussed, along with the types and characteristics of the applied printers. All of the discussed studies are summarized in Table I.

Table I. Reported work on printed oxide thin film transistors.

Authors [ref.]	Materials	Printing	Device performances		
			Mobility (cm^2/Vs)	On/off ratio	V$_{on}$ or V$_{th}$ (V)
Lee et al.[17]	ZIO	Thermal inkjet	7.4	10^4	V$_{on}$ = −26
Kaneda et al.[19]	In$_2$O$_3$	Rheology	10.2	10^5	V$_{on}$ = 0
Lee et al.[22]	SnO$_2$	Thermal inkjet	3.62	10^3	V$_{on}$ = −39
Lee et al.[23]	IZTO	Piezoelectric inkjet	30	10^6	V$_{on}$ = 2
Han et al.[24]	IGO	Piezoelectric inkjet	5.5	10^5	V$_{on}$ = −21
Kim et al.[25]	ZTO	Piezoelectric inkjet	4.98	10^9	V$_{on}$ = −9
Avis et al.[28]	IZTO	Piezoelectric inkjet	114.8	10^7	V$_{th}$ = −0.16
Garlapati et al.[29]	In$_2$O$_3$	Piezoelectric inkjet	126*	2 × 10^7	V$_{on}$ = 0.37
Kim et al.[31]	ZTO	Piezoelectric inkjet	0.58	5 × 10^6	V$_{th}$ = 1.9
Jeong et al.[32]	ZTO	Piezoelectric inkjet	0.58	10^7	V$_{th}$ = 1.7
Kim et al.[33]	IGZO	Piezoelectric inkjet	0.03	5 × 10^4	V$_{th}$ = 6.2
Kim et al.[34]	IGZO	Piezoelectric inkjet	0.055	10^3	V$_{th}$ = −0.5
Wang et al.[35]	IGZO	Piezoelectric inkjet	1.41	4 × 10^7	V$_{th}$ = −0.5
Wang et al.[36]	IGZO	Piezoelectric inkjet	0.82	6 × 10^5	V$_{th}$ = 7
Hennek[37]	IGZO	Piezoelectric inkjet	2.45	9 × 10^5	V$_{th}$ = 21.9
Jeong et al.[38]	IGZO	Piezoelectric inkjet	7.6	10^7	V$_{th}$ = 11.1
Meyers et al.[39]	ZnO	Thermal inkjet	6.1	>10^6	V$_{on}$ = −7
Dilfer et al.[40]	IZO	Flexographic	2.4	5 × 10^7	V$_{th}$ = 4
Choi et al.[41]	IGZO	Gravure	0.81	10^6	V$_{on}$ = 1.35
Eun et al.[42]	ZnO	Transfer	0.49**	10^5	V$_{th}$ = 12
Lee et al.[43]	IZO	EHD	32***	10^3	V$_{th}$ = <2
Lee et al.[44]	ZTO	EHD	9.82	3 × 10^6	V$_{th}$ = 2.16
Jeong et al.[45]	IGZO	EHD	10.4	10^7	V$_{th}$ = 4.1
Dasgupta et al.[46]	In$_2$O$_3$	Piezoelectric inkjet	0.8****	2 × 10^3	V$_{on}$ = 0
Liu et al.[47]	ZnO	Piezoelectric inkjet	0.69	4 × 10^1	V$_{th}$ = 25.5
Noh et al.[48]	ZnO NW	SAP	4	10^4	

EHD: Electrohydrodynamic
SAP: Self-aligned inkjet printing
*The device was performed with polymer dielectric layer
**The performances were measured from the device prior to the transferring
***The device was performed with HfO dielectric layer
****The device was fabricated at room temperature

Since the printed oxide TFTs were first introduced by using metal halide precursor inks, this general solution route drew much attention from the community, encouraging a significant number of studies regarding the solution-processed and printed oxide TFTs by using simple metal salt precursors. As displayed in Table I the printed oxide thin film transistors using this approach have achieved a high level of device performance including high field effect mobility, high current on-off ratio and positive V_{on}. In terms of printing dispersed oxide nanoparticles, the device performances may be limited by the grain boundary formed between nanoparticle interfaces, serving as charge carrier trap sites.

We believe that the maskless and non-vacuum processes will be the mainstream to reduce the manufacturing cost in the future. For thin film transistor applications, metal oxide semiconductors have attracted a lot of panel makers' attention. Compared to conventional amorphous silicon (a-Si) TFTs, amorphous metal oxide TFTs have superior device performance such as higher mobility, better sub-threshold swing, and lower off-state current. Amorphous metal oxide TFTs have an additional advantage on the device uniformity due to the lacks of grain boundary issues in the poly-Si TFTs. Compared with sputtered oxide TFTs, metal oxide TFTs with solution processes have better flexibility and controllability to adjust the composition of chemical solution. From the development progress, 12.1″ AMLCDs and 4″ Flexible AMOLEDs driving by solution-based metal oxide TFTs were demonstrated successfully in 2013 and 2014, respectively.[56,57] Although only the solution-based metal oxide material was coated as a semiconductor layer and the other layers were deposited by PECVDs and PVDs, it is a big step and a good beginning to change the conventional process layer by layer. From an industry perspective, the solution processes, such as printing technologies, have high potential to replace the conventional cluster and photolithography processes. Printing technologies have several advantages including direct patterning, material saving, and non-vacuum process. But some major challenges need to be overcome, such as the film morphology control, the supply of ink/paste materials, overlay accuracy and pattern uniformity. . . etc. The spin-coated oxide TFTs normally exhibited better performances than printed TFTs using the similar inks.[58–60] With advanced printing technique capable of pattering sub micrometer dimension, one major obstacle in achieving high performance printed oxide TFTs may be originated from the poor morphology control caused by non-uniform distribution of droplets under the Maragoni flow. Some additional important examples that require attention for future research and development efforts including the mechanical design of inkjet printing system for the stable delivery of ink droplets on large area substrates and the development of suitable applicators for continuous Roll-to-Roll (R2R) printing to handle the flexible substrates for flexible electronics applications.

References

1. J. E. Lilienfield (1930), U.S. Pat. 1,745,175.
2. O. Heil, U.K. (1935), U.K. Pat. 439457.
3. Y. T. Sihvonen, S. G. Parker, and D. R. Boyd, *J. Electrochem. Soc.* **114**, 96 (1967).
4. P. G. Lecomber, W. E. Spear, and A. Ghaith, *Electron. Lett.* **15**, 179 (1979).
5. E. Fortunato, P. Barquinha, and R. Martins, *Adv. Mater.* **24**, 2945 (2012).
6. J. Y. Kwon, D. J. Lee, and K. B. Kim, *Electron. Mater. Lett.* **7**, 1 (2011).
7. K. Nomura, H. Ohta, A. Takagi, T. Kamiya, M. Hirano, and H. Hosono, *Nature* **432**, 488 (2004).
8. E. M. C. Fortunato, P. M. C. Barquinha, A. C. M. B. G. Pimentel, A. M. F. Goncalves, A. J. S. Marques, L. M. N. Pereira, and R. F. P. Martins, *Adv. Mater.* **17**, 590 (2005).
9. G. Adamopoulos, A. Bashir, S. Thomas, W. P. Gillin, S. Georgakopoulos, M. Shkunov, M. A. Baklar, N. Stingelin, R. C. Maher, L. F. Cohen, D. D. C. Bradley, and T. D. Anthopoulos, *Adv. Mater.* **22**, 4764 (2010).
10. S. Jeong and J. Moon, *J. Mater. Chem.* **22**, 1243 (2012).
11. H. S. Kim, P. D. Byrne, A. Facchetti, and T. J. Marks, *J. Am. Chem. Soc.* **130**, 12580 (2008).
12. H. Sirringhaus, T. Kawase, R. H. Friend, T. Shimoda, M. Inbasekaran, W. Wu, and E. P. Woo, *Science* **290**, 2123 (2000).
13. J. Z. Wang, Z. H. Zheng, H. W. Li, W. T. S. Huck, and H. Sirringhaus, *Nat. Mater.* **3**, 171 (2004).
14. K. E. Paul, W. S. Wong, S. E. Ready, and R. A. Street, *Appl. Phys. Lett.* **83**, 2070 (2003).
15. A. C. Arias, S. E. Ready, R. Lujan, W. S. Wong, K. E. Paul, A. Salleo, M. L. Chabinyc, R. Apte, R. A. Street, Y. Wu, P. Liu, and B. Ong, *Appl. Phys. Lett.* **85**, 3304 (2004).
16. P. Beecher, P. Servati, A. Rozhin, A. Colli, V. Scardaci, S. Pisana, T. Hasan, A. J. Flewitt, J. Robertson, G. W. Hsieh, F. M. Li, A. Nathan, A. C. Ferrari, and W. I. Milne, *J. Appl. Phys.* **102**, 043710 (2007).
17. D. H. Lee, Y. J. Chang, G. S. Herman, and C. H. Chang, *Adv. Mater.* **19**, 843 (2007).
18. F. L. C. L. John Vaught, K. David Donald, D. John Meyer, A. Christopher Tacklind, and H. Howard Taub, U.S., Pat. No. 4,490,728 (1984).
19. H. Braun, U.S. Pat. No. 5,598,196 (1997).
20. K. D. Bardin, U.S. Pat. No. 4,003,311 (1977).
21. John A. Martens, U.S. Pat. No. 5,175,072 (1990).
22. John A. Peterson, Kurt F. F. Feil, Craig D. Lien, John A. Martens, Gary A. Staus, and Gray D. VanderWerff, U.S. Pat. No. 5,279,697 (1994).
23. D. H. Kim, J. H. Ahn, W. M. Choi, H. S. Kim, T. H. Kim, J. Z. Song, Y. G. Y. Huang, Z. J. Liu, C. Lu, and J. A. Rogers, *Science* **320**, 507 (2008).
24. J. H. Ahn, H. S. Kim, K. J. Lee, S. Jeon, S. J. Kang, Y. G. Sun, R. G. Nuzzo, and J. A. Rogers, *Science* **314**, 1754 (2006).
25. J. U. Park, M. Hardy, S. J. Kang, K. Barton, K. Adair, D. K. Mukhopadhyay, C. Y. Lee, M. S. Strano, A. G. Alleyne, J. G. Georgiadis, P. M. Ferreira, and J. A. Rogers, *Nat. Mater.* **6**, 782 (2007).
26. T. Kaneda, D. Hirose, T. Miyasako, P. T. Tue, Y. Murakami, S. Kohara, J. W. Li, T. Mitani, E. Tokumitsu, and T. Shimoda, *J. Mater. Chem. C* **2**, 40 (2014).
27. O. F. Gobel, M. Nedelcu, and U. Steiner, *Adv. Funct. Mater.* **17**, 1131 (2007).
28. J. Z. Wang, J. Gu, F. Zenhausem, and H. Sirringhaus, *Appl. Phys. Lett.* **88**, 133502 (2006).
29. D. H. Lee, Y. J. Chang, W. Stickle, and C. H. Chang, *Electrochem. Solid St.* **10**, K51 (2007).
30. D. H. Lee, S. Y. Han, G. S. Herman, and C. H. Chang, *J. Mater. Chem.* **19**, 3135 (2009).
31. S. Y. Han, D. H. Lee, G. S. Herman, and C. H. Chang, *J. Disp. Technol.* **5**, 520 (2009).
32. Y. H. Kim, H. S. Kim, M. S. Oh, H. J. Kim, J. I. Han, M. K. Han, and S. K. Park, *IEEE Electron. Device. Lett.* **31**, 836 (2010).
33. R. D. Deegan, O. Bakajin, T. F. DuPont, G. Huber, S. R. Nagel, and T. A. Witten, *Nature* **389**, 827 (1997).
34. D. Soltman and V. Subramanian, *Langmuir* **24**, 2224 (2008).
35. C. Avis, H. R. Hwang, and J. Jang, *ACS Appl. Mater. Inter.* **6**, 10941 (2014).
36. S. K. Garlapati, N. Mishra, S. Dehm, R. Hahn, R. Kruk, H. Hahn, and S. Dasgupta, *ACS Appl. Mater. Inter.* **5**, 11498 (2013).
37. S. Jeong, Y. Jeong, and J. Moon, *J. Phys. Chem. C* **112**, 11082 (2008).
38. D. Kim, Y. Jeong, K. Song, S. K. Park, G. Z. Cao, and J. Moon, *Langmuir* **25**, 11149 (2009).
39. Y. Jeong, K. Song, D. Kim, C. Y. Koo, and J. Moon, *J. Electrochem. Soc.* **156**, H808 (2009).
40. G. H. Kim, H. S. Kim, H. S. Shin, B. D. Ahn, K. H. Kim, and H. J. Kim, *Thin Solid Films* **517**, 4007 (2009).
41. D. Kim, Y. Jeong, C. Y. Koo, K. Song, and J. Moon, *Jpn. J. Appl. Phys.* **49**, 05EB06 (2010).
42. Y. Wang, X. W. Sun, G. K. L. Goh, H. V. Demir, and H. Y. Yu, *IEEE Trans. Electron Devices* **58**, 480 (2011).
43. X. W. S. Y. Wang, S. W. Liu, and A. K. K. kyaw, presented at the *IEEE 5th International Nanoelectronics Conference (INEC)*, 2013.
44. J. W. Hennek, Y. Xia, K. Everaerts, M. C. Hersam, A. Facchetti, and T. J. Marks, *ACS Appl. Mater. Inter.* **4**, 1614 (2012).
45. S. Jeong, J. Y. Lee, S. S. Lee, S. W. Oh, H. H. Lee, Y. H. Seo, B. H. Ryu, and Y. Choi, *J. Mater. Chem.* **21**, 17066 (2011).
46. S. T. Meyers, J. T. Anderson, C. M. Hung, J. Thompson, J. F. Wager, and D. A. Keszler, *J. Am. Chem. Soc.* **130**, 17603 (2008).
47. S. Lee, J. Kim, J. Choi, H. Park, J. Ha, Y. Kim, J. A. Rogers, and U. Paik, *Appl. Phys. Lett.* **100**, 102108 (2012).
48. Y. G. Lee and W. S. Choi, *ACS Appl. Mater. Inter.* **6**, 11167 (2014).
49. S. Jeong, J. Y. Lee, S. S. Lee, Y. H. Seo, S. Y. Kim, J. U. Park, B. H. Ryu, W. Yang, J. Moon, and Y. Choi, *J. Mater. Chem. C* **1**, 4236 (2013).
50. S. Dilfer, R. C. Hoffmann, and E. Dorsam, *Appl. Surf. Sci.* **320**, 634 (2014).
51. Y. Choi, G. H. Kim, W. H. Jeong, H. J. Kim, B. D. Chin, and J. W. Yu, *Thin Solid Films* **518**, 6249 (2010).
52. W.-H. L. Chao-Te Liu and Tsu-Lang Shih, *Journal of Nanotechnology* **2012**, 1 (2012).
53. Y. Y. Noh, X. Y. Cheng, H. Sirringhaus, J. I. Sohn, M. E. Welland, and D. J. Kang, *Appl. Phys. Lett.* **91**, 043109 (2007).
54. S. Dasgupta, R. Kruk, N. Mechau, and H. Hahn, *ACS Nano* **5**, 9628 (2011).
55. K. T. Eun, W. J. Hwang, B. K. Sharma, J. H. Ahn, Y. K. Lee, and S. H. Choa, *Mod. Phys. Lett. B* **26**, 1250077 (2012).
56. L.-Y. Lin, W.-Y. Hung, C.-C. Cheng, C.-Y. Liu, and M.-F. Chiang, *SID' 13 Digest*, pp. 783 (2013).
57. L.-Y. Lin, C.-C. Cheng, C.-Y. Liu, M.-F. Chiang, Po-Hsien Wu, Meng-Ting Lee, Chien-Ying Chen, Chih-Cheng Chan, Chen-Chi Lin, and Chih-Hsiang Chang, *SID' 14 Digest*, pp. 252 (2014).
58. S. Y. Han, G. S. Herman, and C. H. Chang, *J. Am. Chem. Soc.* **133**, 5166 (2011).
59. Y. H. Kim, J. S. Heo, T. H. Kim, S. Park, M. H. Yoon, J. Kim, M. S. Oh, G. R. Yi, Y. Y. Noh, and S. K. Park, *Nature* **489**, 128 (2012).
60. M. G. Kim, M. G. Kanatzidis, A. Facchetti, and T. J. Marks, *Nat. Mater.* **10**, 382 (2011).